TWISTER Hand: Underactuated Robotic Gripper Inspired by Origami Twisted Tower

Kiju Lee, Yanzhou Wang, and Chuanqi Zheng

***Abstract*—This article presents a new cable-driven underactuated robotic gripper, called TWISTER Hand. It is designed for adaptable grasping of objects in different shapes, weights, sizes, and textures. Each finger of the gripper is made of a compliant and continuum mechanism inspired by an origami design. This design is converted into a computer-aided design (CAD) model and 3-D printed using flexible and rigid polymer composite materials. Two CAD modeling methods for this design are compared in terms of structural stiffness and durability in the printed outcomes. For each design, two soft materials are used for preliminary evaluation of the material effect in these properties. The best combination of the model and material is selected to fabricate the three fingers of the robotic gripper. Each finger has a single cable routed along the structure. All three cables are tied and actuated simultaneously using a single servo motor to generate closing and opening motions in the gripper. TWISTER Hand's adaptable grasping capability is tested using 36 different objects. The robot's grasping performance under object pose uncertainties is also experimentally tested and analyzed. This compact fully integrated gripper can be attached to a robotic arm for various manipulative tasks.**

***Index Terms*—Underactuated robotic gripper, continuum mechanism, semisoft robotic hand, 3-D-printed robots.**

Manuscript received May 15, 2018; accepted October 29, 2019. Date of publication January 3, 2020; date of current version April 2, 2020. This article was recommended for publication by Associate Editor K.-J. Cho and Editor I.-M. Chen upon evaluation of the reviewers' comments. *(Corresponding author: Kiju Lee.)*

K. Lee was with the Department of Mechanical and Aerospace Engineering, Case Western Reserve University, Cleveland, OH 44106 USA. She is now with the Department of Engineering Technology and Industrial Distribution and the Department of Mechanical Engineering, Texas A&M University, College Station, TX 77843 USA (e-mail: kiju.lee@tamu.edu).

Y. Wang was with the Department of Mechanical and Aerospace Engineering, Case Western Reserve University, Cleveland, OH 44106 USA. He is now with the Department of Mechanical Engineering, Johns Hopkins University, Baltimore, MD 21218 USA (e-mail: ywang521@jh.edu).

C. Zheng was with the Department of Mechanical and Aerospace Engineering, Case Western Reserve University, Cleveland, OH 44106 USA. He is now with the Department of Mechanical Engineering, Texas A&M University, College Station, TX 77843 USA (e-mail: chuanqi.zheng@tamu.edu).

This article has supplementary downloadable material available at http://ieeexplore.ieee.org, provided by the authors. The material consists of a video, showing the robots grasping performance using a variety of objects. This video shows TWISTER Hand's object grasping demonstrations. Objects used in this video include Rubik's cube, paper food container, bag of snack, egg, spring clamp, small cube, plastic candy box, lime, spool of wire, and a piece of fabric. The size of the video is 51.7 MB. Contact Kiju Lee (e-mail: kiju.lee@tamu.edu) for further questions about this article.

Color versions of one or more of the figures in this article are available online at http://ieeexplore.ieee.org.

Digital Object Identifier 10.1109/TRO.2019.2956870

Fig. 1. Underactuated cable-driven robotic gripper with three compliant fingers fully open (left) and closed (right).

I. Introduction

A NEW underactuated robotic gripper, called TWISTER Hand (see Fig. 1), presented in this article consists of three 3-D-printed compliant fingers. The finger mechanism is inspired by an origami twisted tower designed by Mihoko Tachibana. This origami structure is formed by stacking multiple octagon layers together. An n-layer tower requires $24 + 16(n-1)$ origami segments to be folded and assembled. It generates continuous bending, twisting, and linear motions via structural reconfiguration, and its linear extension-to-contraction ratio can reach over 4:1. Utilizing these unique structural properties, twisted towers were used for various robotic applications, including reconfigurable origami wheels [1], a crawling robot [2], and a robotic manipulator arm [3]. In particular, the three-finger robotic manipulator presented in [3] used the hand-folded twisted towers for its arm and fingers, demonstrating object manipulation capabilities. Despite its potentials demonstrated by these works, hand-folded origami exhibits inconsistency in design outcomes and limitations in achievable compliance levels. In addition, the dexterity of human hands poses great challenge in folding complex and miniature origami shapes. Although there have been some efforts to develop automated systems for origami folding, their capabilities were limited to simple folding patterns and thus not suitable for complex origami designs, such as the twisted tower [4], [5].

To preserve the unique structural reconfigurability of the origami design, the surfaces must remain rigid, while the

creases—where bending occurs—must be flexible to enable kinematic motion. 3-D printing using flexible and rigid materials is considered a uniquely suitable method to fabricate such a complex structure. In our recent work, the origami twisted tower was successfully converted into a 3-D-printable computer-aided design (CAD) model (Model I) [6], [7]. While the outcome well preserved the original twisted tower's kinematics and demonstrated technical feasibility of automated fabrication, Model I was too fragile for applications involving frequent external impact or direct physical contact.

Building on our prior work, this article presents a new design method (Model II) for this mechanism with improved structural properties. The new design method was experimentally tested for its durability and stiffness compared to Model I. For preliminary evaluation of material effect, two different soft materials (i.e., TangoPlus and Agilus30) were used to print sample structures for each model. A combination of Model II and Agilus30 resulted in the best performance in terms of durability and stiffness, and was used for fabricating the fingers of the gripper.

Fully assembled, TWISTER Hand is an underactuated semisoft robotic gripper with a single servo motor that generates closing and opening motions simultaneously in all three fingers (see Fig. 1). It is equipped with a wireless communication module (i.e., XBee) for remote control. With the potential of integrating a video camera at the bottom of the finger-mounting chassis, it is possible to achieve fully autonomous grasping operation. The gripper's dexterous and adaptable grasping capabilities via compliant structural properties are demonstrated through physical experiments involving objects in different sizes, shapes, weights, and textures. Further experiments on grasping performance under object pose uncertainties were also conducted, and the results are presented.

Main *technical contributions* of this article include the following:

1) design methods for 3-D-printable foldable structures based on rigid surfaces and flexible creases that are applicable to other designs;
2) experimental evaluation of the effect of design and materials in a 3-D-printed twisted tower structure;
3) development of a highly compact and fully integrated semisoft robotic gripper actuated by a single cable-servo mechanism;
4) experimental evaluation of the gripper's grasping performance for a variety of objects;
5) experimental evaluation of the gripper's grasping capabilities under object pose uncertainties.

II. Related Work

A. Origami in Robotics

Traditional rigid robotic systems have been successfully used for various applications for more than half a century. However, they have not fully met the needs for certain situations, which may involve: 1) unknown, dynamic, and crowded environments; 2) unspecified tasks or workspace; and 3) tasks involving close interaction with humans or fragile objects. Origami structures show unique coexisting properties of flexibility and rigidity, which can lead to breakthroughs in addressing these challenges [8], [9]. Depending on the materials and folding patterns, origami can create a robust yet flexible structure that can endure external impact in crowded environments, while also being safe for close interaction with humans.

In robotics communities, a particular interest has been focused on action origami, referring to the origami designs that can exhibit motion via structural reconfiguration [10]. Engineering applications of action origami include miniature surgical tools [11]–[13], actuators [14]–[17], wheels [18]–[20], antennas [21], [22], batteries and capacitors [23], [24], shelter system design [25], crash boxes and other energy absorption devices [26]–[28], and large space robotic applications [4]. For example, an origami design called magic ball was used for floating aerial robots to provide buoyant force on water when inflated and shrink to reduce energy consumption in the air [29], [30]. Another interesting body of work focused on realizing self-folding in a flat engraved or precut sheet integrated with shape memory alloys (SMAs) or shape memory polymers [31]–[35]. While most of these existing works focus on origami-*based* designs, i.e., converting from a 2-D material/structure to a 3-D mechanism, TWISTER is *inspired* by origami but no longer an origami design. It is a 3-D configurable structure.

B. Soft Robotic Hands

Advancement in synthetic materials has enabled engineers to use soft materials in the robots, aiming to reduce mechanical and algorithmic complexities [36]. Due to dexterity required for object manipulation, in particular for irregular or fragile objects, soft robotic grippers have opened a new era in the field. Inspired by an octopus arm, a long soft structure, typically actuated by pneumatic devices [37] or SMA artificial muscles [38], could act as both the manipulator and the grasper at the same time. Another interesting design of a soft robotic hand is a ball-shaped universal gripper [39], [40]. Built with a granular material, it can adapt to shapes of objects and change its stiffness to grasp. Another recent soft robotic gripper consists of a main frame with two identical 3-D-printed compliant fingers, which are actuated by a gear motor on a moving platform [41]. RBO Hand 2 is equipped with five fingers using PneuFlex actuators demonstrating dexterous and compliant grasping capabilities [42]. With its multiple-degree-of-freedom (DoF) design, this robot achieved 31 out of 33 postures from human grasp taxonomies.

Many existing soft robotic grippers are actuated by pneumatic-based actuators and typically exhibit robust grasping with relatively low control complexity [42]–[46]. Pneumatic-based actuation is often combined with force-based sensors to control the contact forces during object grasping [42], [47], [48]. Some recent works showed improved grasping performance by implementing tunable stiffness in soft fingers by adjusting pressure in double-sided chambers [49], additional suction force by arranging gecko-inspired adhesives on finger surfaces [50], and finger topology optimization [51], [52]. In spite of their technical advantages (i.e., high load bearing and simple control), pneumatic actuation requires bulky accessories,

which are not desirable for compact fully integrated/embedded applications.

C. Underactuated Cable-Driven Robotic Grippers

An underactuated robotic gripper aims to achieve adaptable object grasping at low cost and low complexity [53]. It often combines soft materials with cable-driven actuation in order to overcome lack of DoF via structural compliance. A "backbone" structure is commonly employed for such mechanisms. This design consists of two layers: a rigid layer on the back serving as bones and a soft layer in front connecting these bones. Given objects with specific shape and size, the fingers provide sufficient grip force, limited only by motor torque and finger material strength [54]–[56]. Some other designs include underactuated robotic fingers using individual phalanges connected by flexible joints based on either pulley–spring couples [57] or shape deposition manufacturing (SDM) joints made from a viscoelastic flexure material [58]. These finger designs allow the robotic grippers to achieve stable precise object grasping by topology optimization of phalange shape [59]. By combining series-elastic actuation and individual joint locking, the maximum pullout forces could be increased [60], [61]. By installing rotatable hubs for specific fingers, in-hand repositioning tasks could also be achieved [62].

The primary difference of TWISTER Hand from existing underactuated soft robotic grippers is its compliance achieved by actively controlled bending and passive twisting in the fingers. The design features rotational symmetry; thus, maintains the same physical contact with an external object even when the finger is twisted. Such an additional degree of compliance makes it effective in fragile and irregular object grasping. In addition, its well-defined kinematics enables potential applications in precise motion control. While the current robot uses a single servo motor to actuate the cables in all three fingers, achieving a higher DoF is also feasible via alternating cable-routing schemes and using multiple actuators.

III. Design and Evaluation of the TWISTER Mechanism

TWISTER Hand consists of three fingers that are based on the TWISTER (TWISted TowEr Robot) mechanism [6], [7]. The structural properties of TWISTER are summarized as follows.

1) *Continuum:* Bending, twisting, and linear motions are achievable via a structural reconfiguration.
2) *Compliant:* Structural flexibility allows shape deformation in response to external forces. The level of compliance may be customized by selecting materials with desired flexibility.
3) *Reconfigurable:* It can exhibit more than one control mode and be embodied into different types of robots.
4) *Scalable:* It achieves scalability in two aspects–physical scalability by selecting dimensions and the number of layers and kinematic scalability by selecting a specific regular polygon which determines the kinematic ranges of motion.

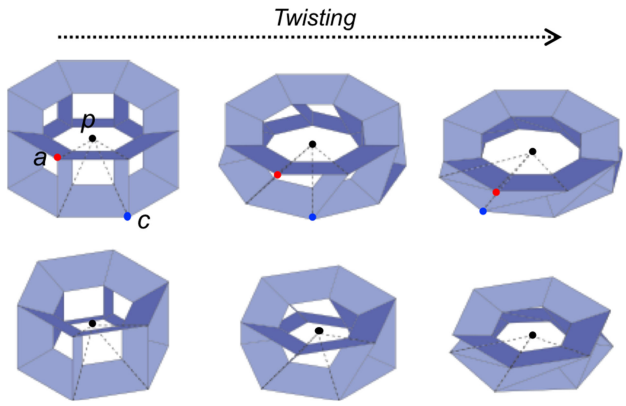

Fig. 2. Twisting motion in a single layer of (top) the octagon-based tower and (bottom) a hexagon-based tower.

A. Kinematics of the TWISTER Mechanism

For better understanding of the mechanism, kinematics of the TWISTER mechanism is briefly reviewed here [3], [7]. A special geometric construct of the twisted tower allows linear and bending motions via twisting in each layer. In the origami twisted tower design, each layer consists of eight interconnected cells, where each of them is formed by four congruent isosceles trapezoids. The extension lines of the nonparallel edges of the trapezoids coincide at a single point P, i.e., geometric centroid, allowing the layer to fully collapse by twisting [see Fig. 2(top)]. This original design uses regular octagon as the base geometry, resulting in $-\pi/4+\epsilon_\theta \leq \theta \leq \pi/4-\epsilon_\theta$, where θ is the twist angle and ϵ_θ is associated with a small unreachable angle due to wall thickness in the tower.

This unique geometric property has inspired kinematic diversification of the design. Any regular polygon with m sides, where $m \geq 3$, can be selected for a desired range of twist angle, such that $-2\pi/m+\epsilon_\theta \leq \theta \leq 2\pi/m-\epsilon_\theta$. Fig. 2(bottom) shows a design using a regular hexagon as the base geometry. Selection of a specific polygon not only determines the range of twist angle (θ), but also defines the maximum bending angle (ϕ) within the layer. Such properties makes TWISTER a geometrically well-defined mechanism, whose kinematic workspace is uniquely determined by the selected geometry and physical dimensions (e.g., edge length and number of layers in a tower).

Virtual planes defined by the outer edges of the polygon do not change during twisting or bending. This allows us to describe the structure configuration using traditional rigid-body kinematics. Fig. 3 shows kinematic parameters used to describe transformation from the bottom to the top plane in the ith layer. The coordinate frame is attached at the center of the bottom plane [see Fig. 3(a)]. It is assumed that the linear displacement between the top and bottom planes within a layer is first applied, and then, bending toward a specific direction takes place. As shown in Fig. 3(b), the twisting angle θ_i results in a screw motion in keeping the top and bottom planes parallel to each other. The resulting linear distance between the top and bottom planes is given by

$$l_i = h - \frac{mh}{2\pi}|\theta_i| \tag{1}$$

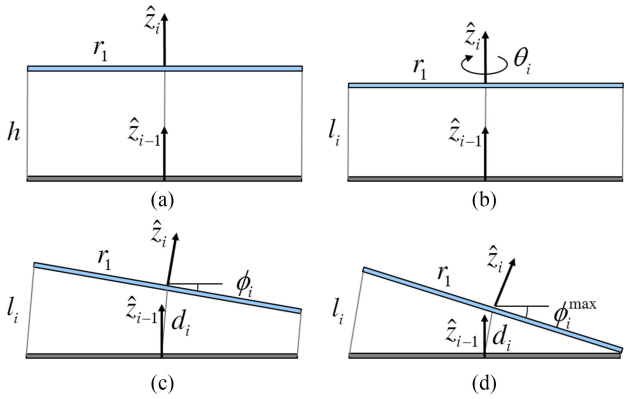

Fig. 3. Side views of a single tower layer, along which the bending occurs. (a) When the layer is fully stretched, the distance between the top and bottom layers is the same as the length of a side of a selected polygon. (b) Twisting the top layer by θ_i results in a linear displacement, l_i. (c) While keeping l_i constant on one side, bending (ϕ_i) is applied to the other side. (d) Maximum bending $\phi_i^{\max}$ is achieved when the top and bottom plates coincide with a small distance between the two caused by structure thickness, ϵ_d. Figures are adopted and modified from [3].

where h is the height of the vertical walls as well as the length of a side for an m-sided regular polygon. When $\theta_i = \pm(2\pi/m - \epsilon_\theta)$, i.e., the top and bottom planes are fully collapsed, l_i becomes the minimum, and this value is calculated as

$$\epsilon_d = h - \frac{mh}{2\pi}\left(\frac{2\pi}{m} - \epsilon_\theta\right). \tag{2}$$

Bending between the top and bottom planes may occur toward any direction, such that $0 \le \alpha_i < 2\pi$. The bending angle ϕ_i is limited to $0 \le \phi_i \le \phi_i^{\max}$, where $\phi_i^{\max}$ can be obtained by

$$\phi_i^{\max} = 2\sin^{-1}\left(\frac{l_i - \epsilon_d}{4r_1}\right). \tag{3}$$

r_1 is a design parameter, i.e., the radius of the inscribed circle for the outer polygon. The translation along the z-axis from the $(i-1)$th frame to the ith frame can then be calculated by

$$d_i = l_i - 2r_1 \sin\left(\frac{\phi_i}{2}\right). \tag{4}$$

Fig. 3(c) and (d) illustrate bending applied toward $\alpha_i = 0$. When it reaches $\phi_i^{\max}$, one side maintains the distance between the top and bottom plates at l_i, while the other side results in the minimum distance, ϵ_d. Finally, the corresponding transformation matrix using the above parameters can be calculated by [7]

$$T_i = \begin{bmatrix} R_i & \vec{p}_i \\ \vec{0}^T & 1 \end{bmatrix} \tag{5}$$

where

$$R_i = \begin{bmatrix} s\beta_i s\alpha_i + c\beta_i c\alpha_i c\phi_i & c\beta_i c\phi_i s\alpha_i - s\beta_i c\alpha_i & c\beta_i s\phi_i \\ s\beta_i c\alpha_i c\phi_i - c\beta_i s\alpha_i & c\beta_i c\alpha_i + s\beta_i c\phi_i s\alpha_i & s\beta_i s\phi_i \\ -c\alpha_i s\phi_i & -s\alpha_i s\phi_i & c\phi_i \end{bmatrix}$$

and

$$\vec{p}_i = \begin{bmatrix} d_i s\frac{\phi_i}{2} c\beta_i \\ d_i s\frac{\phi_i}{2} s\beta_i \\ d_i c\frac{\phi_i}{2} \end{bmatrix}.$$

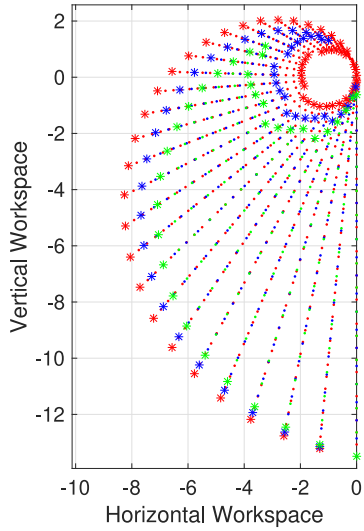

Fig. 4. Kinematic workspace of three ten-layer TWISTERs, using octagon (green), hexagon (blue), and square (red) as the base geometry with a fixed bending direction, $\alpha = \pi$. The top end of the tower is fixed at (0, 0), and the reachable positions of the bottom end of the towers are plotted. Boundaries are marked with "⋆."

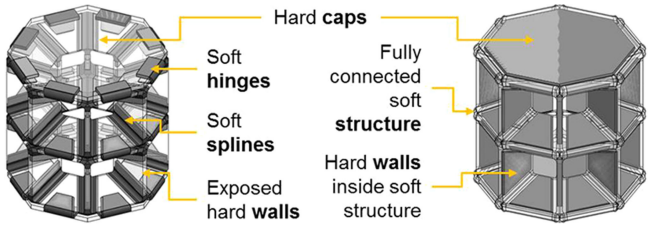

Fig. 5. Two CAD models. (Left) Model I. (Right) Model II.

For n layers, the composite transformation is given by $T = \Pi_{i=1}^{n} T_i$. Depending on how the structure is actuated, the composite transformation can be further simplified as demonstrated for the octagon-based TWISTER structure in [3]. Fig. 4 shows a 2-D plot of kinematic workspace of a ten-layer TWISTER ($n = 8$) based on octagon ($m = 8$, shown in green), hexagon ($m = 6$, shown in blue), and square ($m = 4$, shown in red) as the base geometry. Specific parameter values used are $h = 1.7$, $\epsilon_d = 0$, and $r_1 = 1$. We note that the fingers used the mechanism with $m = 6$ and $n = 8$, shown in blue in Fig. 4.

B. CAD Modeling

CAD modeling first uses four design parameters to determine the overall dimensions [7]:

1) m: the number of edges of a selected regular polygon, i.e., $m \ge 3$;
2) n: the number of layers in a tower;
3) r_1: the radius of the inscribed circle for outer polygon;
4) r_2: the radius of the inscribed circle for inner polygon.

Based on these four parameters, two different CAD models of TWISTER (i.e., Models I and II) are presented (see Fig. 5). Model I used four distinct groups of components: rigid *walls* (i.e., trapezoidal-shaped components that support

the structure), soft *hinges* that connect adjacent walls between two layers, soft *splines* that connect three adjacent walls, and rigid *caps* that provide flat covers for both ends of the tower structure [see Fig. 5(left)]. To print out the entire mechanism as a single structure without requiring subsequent assembling, grooves were created in rigid components to result in a secure interface between soft and hard components during the printing process. Walls are connected to hinges and splines with sufficient clearance to ensure unhindered movement. The cap provides a flat surface for interfacing with other hardware components, such as control modules and sensors. Based on these four components, a fully assembled twisted tower was designed in a commercial CAD software, as shown in Fig. 5(left). Flexible components are shown in black and rigid in translucent. While this model successfully demonstrated the feasibility, the structure was not durable for a long-term use, and repeated bending inevitably resulted in cracks in soft components, particularly in the splines where the most significant deformation occurs.

Model II takes a different design approach. As shown in Fig. 5(right), instead of exposing all rigid components as in Model I, the walls and caps in the previous design were converted into rigid inserts in a single soft enclosure, which takes on the combined role of hinges and splines as in Model I. This design modification was intended to better preserve the printed model by removing the sudden transition from flexible to rigid material, especially for the splines where most cracks initiate. In addition, this design change opens up the possibility of utilizing the soft material, not only for its flexibility, but also for the friction it provides to interact with the environment or objects. Compared to Model I, the flexible enclosure in Model II now constitutes a much larger portion of the design, while the walls and caps still play a critical role when the structure reconfigures, as they geometrically restrict the deformation in flexible components and guide the kinematic motion in the structure. Depending on the need, the size of the rigid wall inserts can be easily adjusted to vary the amount of deformation allowed in each layer. For example, smaller walls would allow more deformation in the soft component, which, in turn, would result in higher overall flexibility in the structure.

C. Sample Preparation and Fabrication

To compare the two design methods, two-layer samples using Models I and II were 3-D printed for structural stiffness and robustness testing. While material engineering and optimization is not within the scope of this article, two different soft materials (i.e., TangoPlus and Agilus30) were used for each design to observe the material effect. Considering the expected "folding" motions at splines and hinge areas, two most flexible materials among all available materials from the manufacturer were selected. Table I shows properties of these two materials [63]. Agilus30 appears to have higher tensile strength and tear resistance while also being more flexible. These property differences are also verified via stiffness and fatigue testing presented later in this subsection.

TABLE I
MATERIALS DATA FOR THE TWO SELECTED SOFT MATERIALS

	Unit	TangoPlus	Agilus30
Tensile strength	Mpa	0.8-1.5	2.4-3.1
Elongation at break	%	170-220	220-240
Shore A hardness	Scale A	26-28	30-35
Tensile tear resistance	kg/cm	2-4	5-7

TABLE II
MODEL TYPE, SOFT MATERIAL, VOLUME (cm^3), AND BUILD TIME (HOUR) FOR THE FOUR TWO-LAYER SAMPLES

Sample no.	CAD Model	Material	Volume	Build Time
1	I	TangoPlus	22.24	6.47
2	I	Agilus30	22.24	6.47
3	II	TangoPlus	22.84	5.83
4	II	Agilus30	22.84	5.83

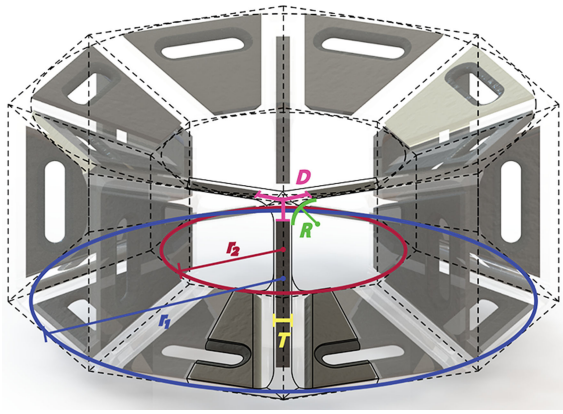

Fig. 6. Four sets of parameters that define the dimension of the spline structure: r_1, r_2, D, and R. These four parameters determine the shape and volume of the spline.

Four samples used for testing include Model I using TangoPlus (flexible) and VeroWhite (rigid), Model I using Agilus30 (flexible) and VeroWhite, Model II with TangoPlus and VeroWhite, and Model II using Agilus30 and VeroWhite. These samples were fabricated by the Objet350 Connex3 3-D printer from Stratasys. Total volume and printing time for each two-layer sample are shown in Table II. To compare the two design methods and soft materials, other possible variables were kept as consistent as possible between the two models. Four sets of key parameters, shown in Fig. 6, are identified and explained as follows. The four samples were created while keeping the following parameters exactly the same.

1) r_1 and r_2: the radius values of the inscribed circles for the outer and inner structures, respectively. The distance between two corresponding vertices of the two octagons defines the longitudinal length of the splines.
2) Wall-to-wall distance (D): a spline connects three adjacent walls. In Model I, the spline is an individual component that bridges the gaps between the rigid walls; in Model II, the spline is inseparable from the holistic soft enclosure, yet the region in between three adjacent walls is essentially filled by the spline. The wall-to-wall distance defines the transverse length of the splines.

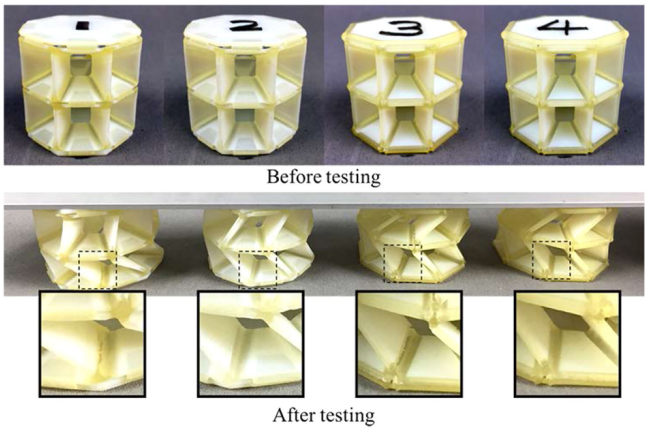

Fig. 7. Four samples (top) before and (bottom) after 1000 sinusoidal cycles: Samples 1 and 3 using TangoPlus showed visible damages on spline areas, while Samples 2 and 4 using Agilus30 remained intact.

3) Spline thickness (T): the thickness of the spline gives the third dimension that is needed to determine the total volume of a basic spline.
4) Fillet radius (R): fillets are created uniformly at locations of right angles on the splines. It has been observed that while the fillets alleviate stress concentration during loading, their size will affect the flexibility of the structure during twisting and bending.

D. Stiffness and Durability Testing

The 3-D-printed samples were tested with an Instron servo-hydraulic testing machine (Model 8501) to measure stiffness and fatigue in the printed structures due to repeated compression over time. A total of 1000 sinusoidal cycles with 1-Hz frequency and 15-mm amplitude (30-mm stroke) were induced on each sample, and a 250-lb load cell was used to record relevant data at each cycle. During testing, the room temperature is 22.8 °C with 13% relative humidity.

Fig. 7 shows the samples before and after testing. Fig. 8 shows the stiffness and fatigue testing results. The effect of different CAD modeling methods was examined by comparing Samples 1 and 3 and Samples 2 and 4. After 1000 cycles, Sample 1 suffered 34.7% and 39.5% decrease, while Sample 3 showed 20.0% and 33.5% decrease in loading and unloading stiffness values, respectively. Sample 2 showed 11.9% and 20.1% decrease, while Sample 4 experienced 8.14% and 18.8% decrease in loading and unloading stiffness values, respectively, after 1000 cycles. In addition, for each soft material, Model II showed higher overall stiffness and suffered less from fatigue than Model I. In terms of materials, TangoPlus shows great variability, as its stiffness properties changed throughout the experimental cycles and resulted in visible damages. Agilus30, on the other hand, behaved much more consistently and remained intact after testing. Based on these results, Model II with Agilus30 was selected for fabricating the fingers of the presented robotic gripper.

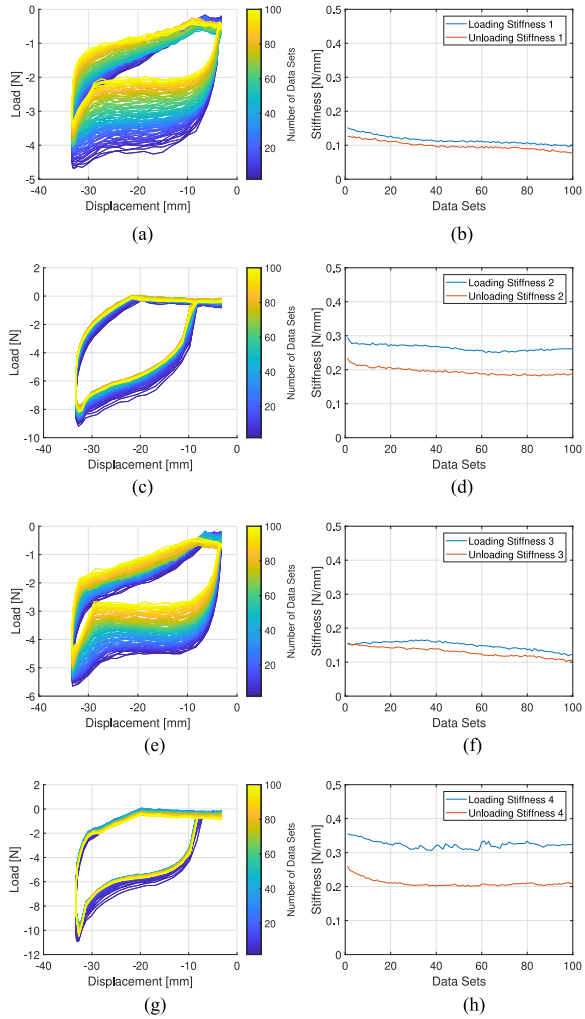

Fig. 8. Results from the loading and unloading tests for the four samples. (a) Model I with TP: Stiffness. (b) Model I with TP: Fatigue. (c) Model I with AG: Stiffness. (d) Model I with AG: Fatigue. (e) Model II with TP: Stiffness (f) Model II with TP: Fatigue. (g) Model II with AG: Stiffness. (h) Model II with AG: Fatigue.

IV. Development of a Robotic Gripper

TWISTER Hand is a one-DoF robotic gripper with a simple closing/opening operation. Taking advantage of their compliance, the fingers can effectively deform around an object—which may be irregular and/or fragile—without force feedback. The special geometric design allows the fingers to maintain proper contact with the object even when the fingers are twisted to adapt to the object's shape. The three fingers are evenly placed in a circular pattern on a chassis, which contains a pulley mechanism for pulling and releasing the cables from the fingers using a single servo motor. Fingers, chassis, and pulley were 3-D-printed using Objet350 Connex3.

A. Fingers

Each finger was 3-D printed using the Model II design with $m = 6$, $n = 8$, $r_1 = 28.39$ mm, and $r_2 = 12.12$ mm. Each finger weighs about 13 g. The total length is 129.95 when fully

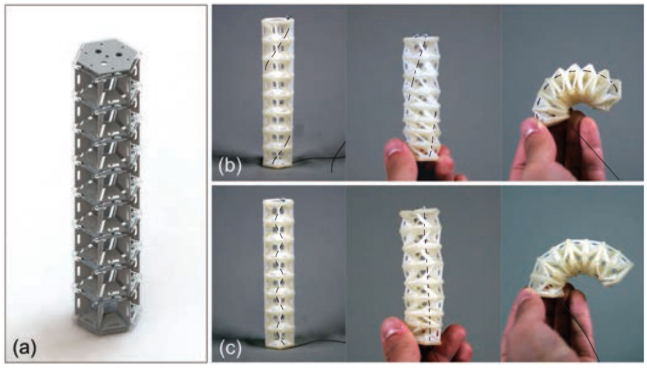

Fig. 9. Final CAD drawing and printed outcome. (a) CAD model of TWISTER with embedded holes for routing cables. (b) Printed structure with cables routed diagonally. (c) Structure with cables routed in a zigzag pattern.

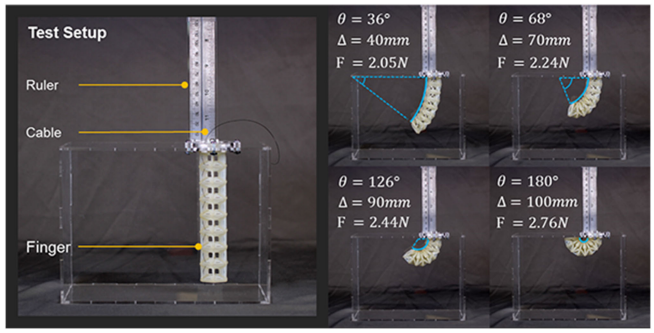

Fig. 10. Bending angle versus pulling distance and pulling force. The test set up included a clear box frame with a ruler. The cable from the finger was connected to a spring pull force gauge and pulled from the top.

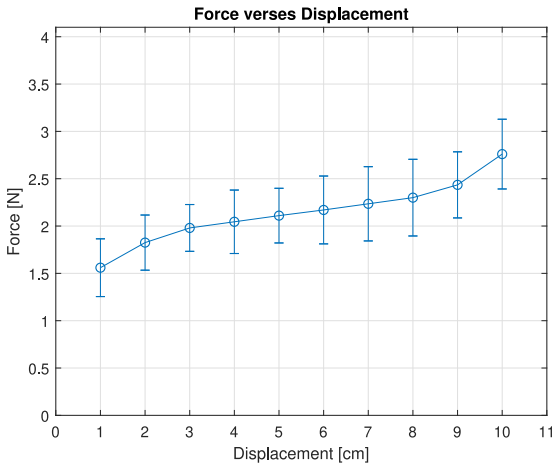

Fig. 11. Pulling force [N] versus pulling distance [cm].

extended and 32.00 when fully contracted. Slots and holes were created on the walls and top and bottom caps of each finger for routing cables. The fingers were fabricated using VeroWhite (rigid) and Agilus30 (soft), which were also used in the two-layer samples for fatigue and stiffness testing.

Fig. 9(a) shows the actual CAD model used for the finger, and Fig. 9(b) and (c) shows how cables can be routed to generate linear and bending motions. In Fig. 9(b), two cables were routed diagonally resulting in continuous twisting during linear contraction. In Fig. 9(c), the cables are routed in a zigzag pattern, resulting in pure translation between the bottom and top layers for a tower with an even number of layers. For the presented robotic gripper, a single cable was routed in the zigzag pattern for each finger to generate bending motion.

The entire fabrication process for each finger takes around 8.5 h from start to finish. Only minimal human intervention ($\leq$10 min) is required during this process, such as setting up the file and machine for printing and placing and retrieving the printed structure from the lye bath. Advantages of Model II over Model I were also observed in the fabrication process: Model I often showed cracks or premature deformation in its components after removal of the support material, while Model II resulted in significantly more consistent outcomes with the same fabrication equipment and procedures.

B. Cable-Driven Actuation and Grasping Force

For the conceived robot embodiment, one DoF is considered sufficient for simple closing and opening operations. Validation of cable-driven actuation was focused on testing pulling force required for bending the structure and contact force generated by the TWISTER mechanism.

For the bending experiment, a simple acrylic testbed was constructed. As shown in Fig. 10, the finger with a cable was installed on the box frame. A ruler was mounted on the top of the frame to measure the pulling distance. The end of the cable was tied to a spring pull force gauge and pulled vertically from the top. Pulling force, pulling distance, and bending angle were measured simultaneously. Ten readings were recorded at each distance, and the average and standard deviation were calculated. Fig. 11 shows that the pulling force gradually increased from 1.55 to 2.75 N, while the pulling distance increased from 1 to 10 cm. The circle and bar length indicate the average and standard deviation, respectively, at each distance point.

Another set of experiments aimed at measuring the grasping force that can be exerted on an object. Due to the complex geometry of TWISTER, the contact surface between an object and the finger is not well defined; in addition, its compliant nature presents challenges in measuring the grasping force accurately. However, even rough estimation of such force generated by each finger is important for examining its potential grasping capability. As a step toward evaluating the feasibility of cable-based actuation, a simple experimental protocol was developed and explicated here.

For this experiment, a force-sensitive resistor (FSR) pad was used. Calibration of the FSR was performed by placing it on a weight scale: 1) place an FSR with a thin leather pad on the scale and set it to 0 N; 2) use the TWISTER finger to exert force on the FSR; 3) compare readings from the weight scale and FSR readings; and 4) an offset is added for calibration. The force from the fingers remained within 0–5 N, which simplified calibration. It is also noted that recalibration may be required for different environmental settings or as the system ages.

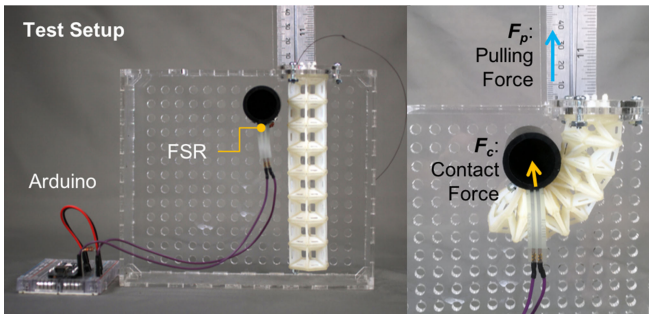

Fig. 12. Experimental setup for measuring resultant force applied to an object by the TWISTER finger.

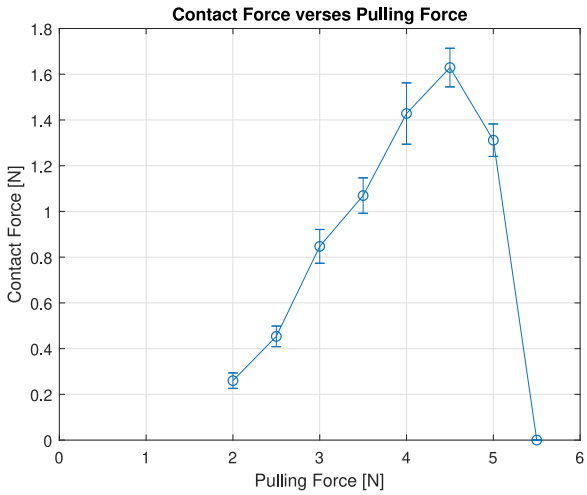

Fig. 13. Pulling force versus contact force [N]. At over 4.5 N of pulling force, the finger started slipping off the sensor attached on the cylinder.

On a testbed shown in Fig. 12, a 25-mm-diameter cylinder was mounted on the back wall, and a FSR pad was attached to the surface of the cylinder in order to measure the induced force upon contact. Because of the small and irregular contact surface between the cylinder and the finger, a thin leather pad was attached on top of the FSR in order to better distribute the contact force on the sensor surface—without this pad, the FSR was not able to register contact force data reliably. Pulling forces ranging from 2 to 5 N with 0.5-N increments were applied on the cable, and the FSR readings were recorded.

To ensure a relatively accurate representation of the actual grasping performance, FSR readings were continuously measured, while the pulling force gradually increases until the finger slips off the cylinder and no longer contacts the surface of the FSR. As shown in Fig. 13, the slipping phenomenon is particularly noticeable when the pulling force exceeds 4.5 N, upon which the finger could barely remain in a statically sound position relative to the sensor. At 5.5 N, the finger completely slips off the sensor, and therefore, no contact force could be measured by the FSR. In between 2 and 4.5 N of the pulling force by the cable, the resulting contact force increased from 0.26 to 1.63 N. The circle and bar length indicate the average of 100 FSR readings and its standard deviation at the contract surface given each pulling force.

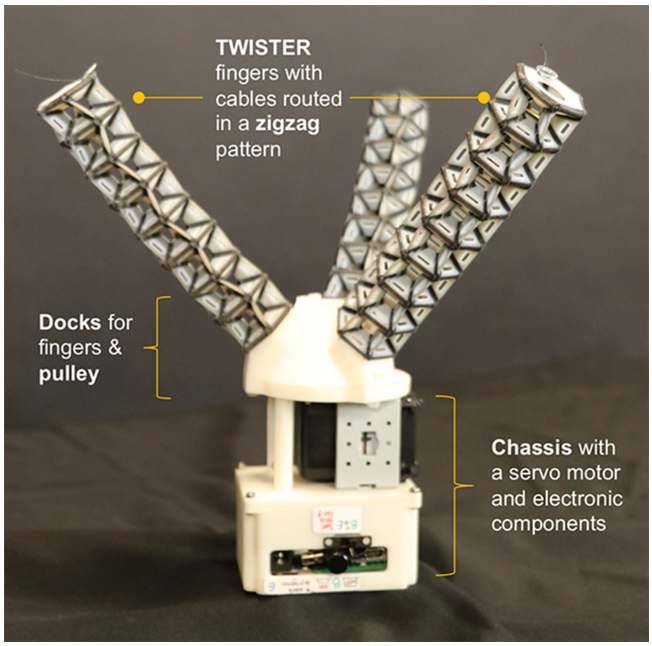

Fig. 14. Fully assembled TWISTER Hand with the main chassis and three fingers, each with a cable.

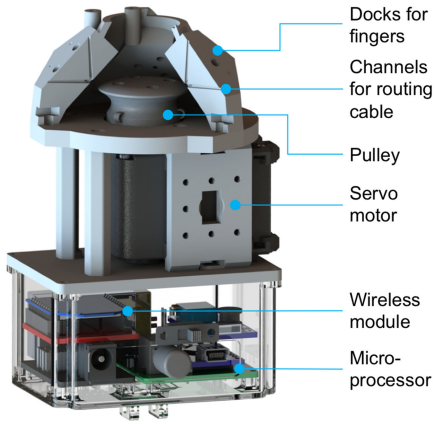

Fig. 15. Main chassis contains a microprocessor, battery, power switch, mini USB port, XBee module, servo motor, pulley mechanism, and docks for the fingers and cables.

C. Hardware Integration

TWISTER Hand is a compact, fully integrated robotic gripper, using a single servo to simultaneously actuate the three cables on the fingers to generate closing and opening motions (see Fig. 14). It is noted that while the current embodiment focuses on the simplest actuation solution with a minimum DoF, these fingers can be independently controlled by using three motors or each finger may exhibit more than one DoF with two or more actuators. The chassis design includes more than one channel for cables to go through, if a higher DoF or a different routing pattern is desired. The fully integrated gripper weighs about 2.75 N.

As shown in Fig. 15, the gripper's chassis includes a microprocessor (i.e., Arduino Nano), a wireless communication module (i.e., XBee), two rechargeable lithium polymer batteries (350 mAh; 3.7 V), a servo motor, and a pulley. The chassis also

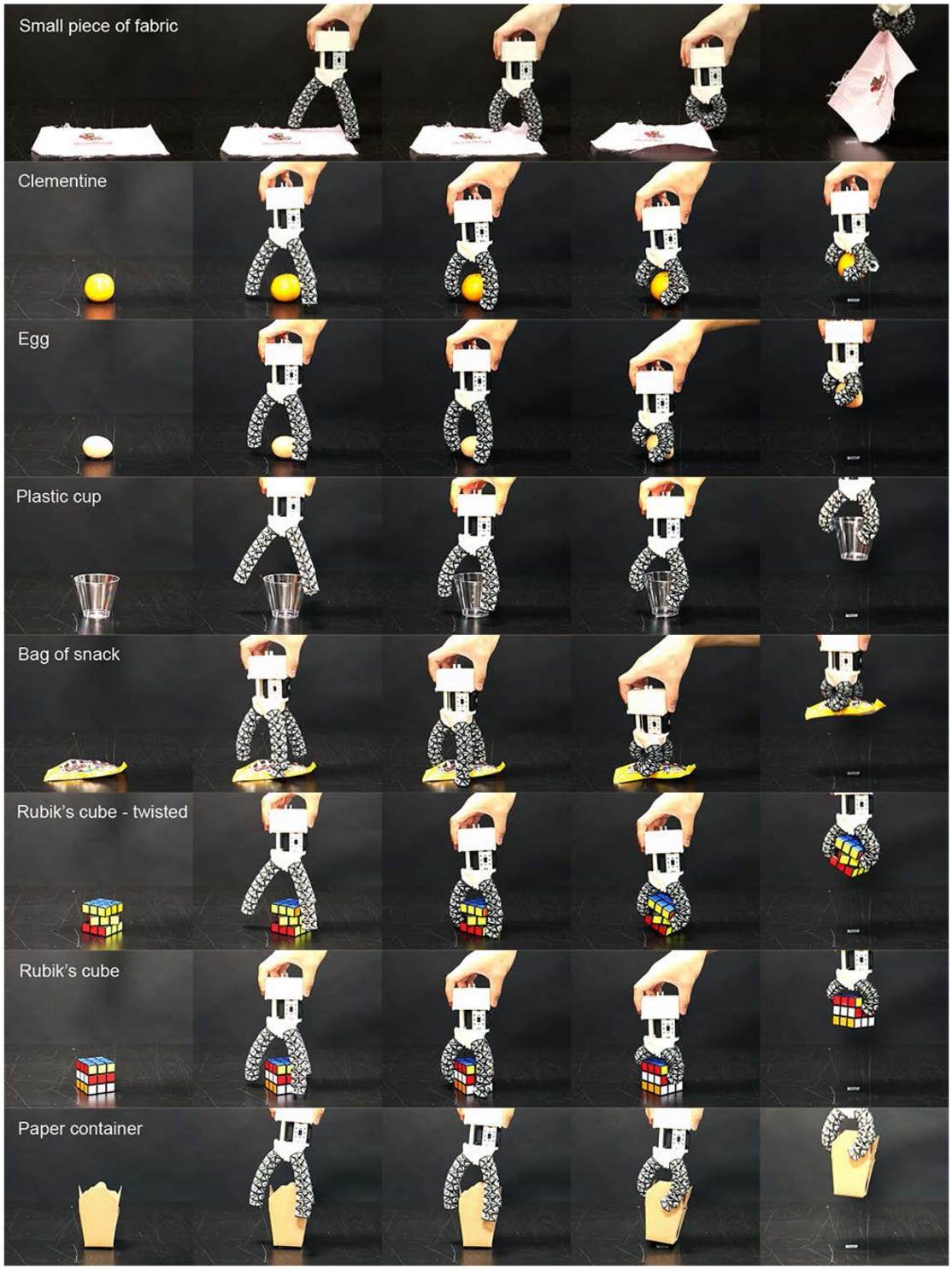

Fig. 16. Video-captured images from object acquisition experiments for eight selected objects.

has an ON/OFF switch and a mini USB port for programming and charging. The chassis without the fingers weighs about 2.36 N and is $63.55 \times 87.86 \times 77.42$ mm^3 in size. The remote controller also has an XBee module with an integrated circuit to send control commands to the gripper. Wireless operation involves two buttons on the remote controller: one for opening and the other for closing motions in the fingers. The current hardware design can also support additional sensors, such as a camera.

V. Grasping Performance Evaluation

Experimental evaluation focused on examining the following two characteristics:

Fig. 17. Thirty-six objects used in our experiments. Colored boxes on each object indicate the number of successful grasping out of three trials: green (3/3), yellow (2/3), orange (1/3), and red (0/3). Objects with two colored boxes were tested in two different orientations.

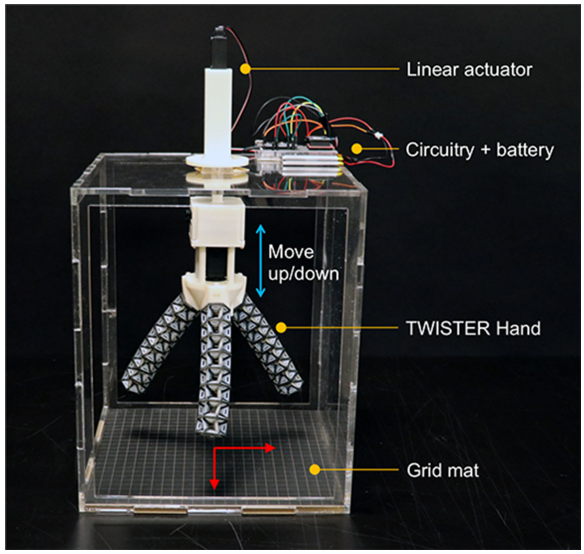

Fig. 18. Experimental setup for grasping test for object's positional and orientational uncertainties.

1) grasping performance in terms of object acquisition and retention capabilities;
2) grasping performance under object's positional and orientational uncertainties.

While the presented gripper can be attached to an articulated robotic arm for fully autonomous object grasping and manipulation, this early stage evaluation focused on validating the effectiveness of the semisoft fingers on grasping objects with different sizes, shapes, and textures through passive deformation and without sensor-based control. To do so, the gripper was moved by a human hand to the target object and remotely controlled for opening and closing of the fingers.

A. *Basic Grasping Performance*

The basic grasping capability was examined by using 36 objects with various shapes, sizes, weights, and textures, such as packaged snacks, fruits, daily accessories, and small toys. A complete list of objects and their specifics can be found in Table III.

Object grasping capability was tested by acquiring an object placed on a flat smooth table and holding it for about 10 s. For each object, three trials were performed, and successful grasping was counted. Fig. 16 shows selected video-captured images of this test for eight different objects. To focus on the gripper design itself, we took the liberty of approaching and grasping from various poses, which is deemed to be appropriate for each object. Among the 36 objects employed, the gripper could successfully grasp 28 objects reliably (3/3 success rate) and 31 objects at least two out of three trials. A small subset of objects, including a plastic bottle, paper/plastic cups, paper food container, wire spools, and tapes, was tested for two different orientations (i.e., vertical and horizontal). Fig. 17 shows all 36 objects used in this test, with colored boxes indicating successful acquisition rates (i.e., green: 3/3 success trials, yellow: 2/3, orange: 1/3, and red: 0/3). Objects with two colored boxes are ones tested for two different orientations.

The results indicate that while the gripper was able to successfully grasp most of these objects, the object's geometrical shape is one of the main factors affecting the success rate. In short, the gripper can easily acquire objects that have distinct convex shapes at a location reasonably high above a flat surface, but it struggles when the object does not have this "desired" shape. For example, the gripper could easily acquire the Rubik's cube, while its layers were not aligned, yet it failed at times to grasp it when the layers are perfectly lined up. In addition, the gripper could not grasp a pencil, banana, or tape when they were laid flat on the table surface; however, it could acquire these same objects when they were slightly elevated above the surface.

B. *Grasping Performance Under Uncertainties*

TWISTER Hand's grasping performance under object pose uncertainties was examined via a structured experimental setup benchmarking the study design presented in [47]. As shown in Fig. 18, the gripper was installed on a frame and attached to a linear actuator in an upright position. The linear actuator moves the gripper up and down for top grasp. At the bottom of the frame, a 10-mm grid pattern was engraved. The experiment procedure is programmed as that the linear actuator first lowers the gripper to approach the object from the top and then closes the fingers for 2 s. The linear actuator then raises the gripper and stays in the position for 10 s. A successful grasp is determined at this stage as whether the gripper can grasp and hold the object for 10 s. After that, the gripper is lowered and opened to release the object, and finally, the gripper is brought back to its initial position for the next test.

A small cube ($38 \times 38 \times 38$ mm^3) made from matboard was used for this experiment for ease of determination of its position and orientation. The cube was first placed right underneath the center of the gripper. The grasping test involves moving the gripper in the aforementioned sequence three times for each

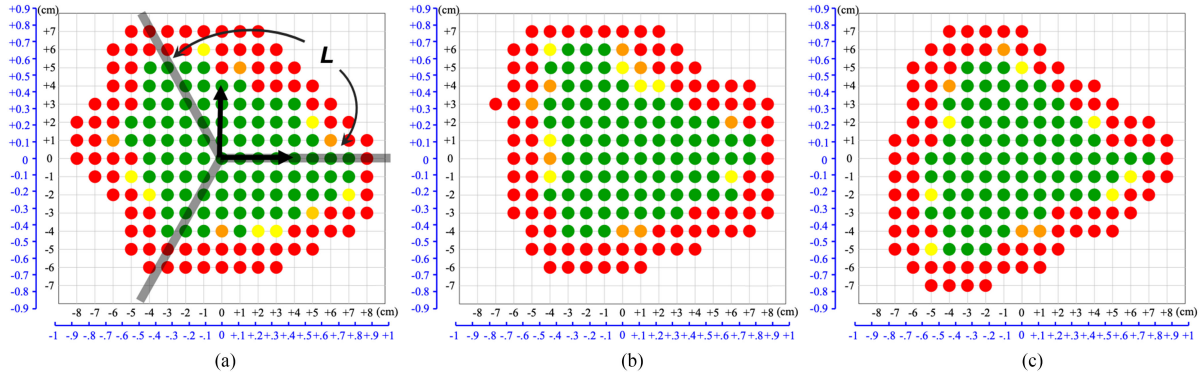

Fig. 19. Grasping performance results under object's positional and orientational uncertainties using a small cube ($38 \times 38 \times 38$ mm^3) placed at different positions on a 10-mm-resolution grid with (a) 0° (projected finger configuration shown with three gray lines), (b) 30°, and (c) 60°.

orientation $(0, \pi/6, \pi/3)$ of the cube at each location on the grid mat. Considering the rotational symmetry of the cube, these three distinctive orientations represent the entire orientational uncertainties at the resolution of $\pi/6$. The test was repeated for all reachable positions on the grid.

Fig. 19 shows the results using the same color coding as in Fig. 17. The capture areas for 100% successful grasping were 86, 81, and 85 cm^2 for the cube placed at 0°, 30°, and 60°, respectively. When including $\geq 67\%$ success rate (2/3 success), the capture areas expand to 93, 88, and 86 cm^2. The capture area is geometrically linked to the size of the gripper/fingers relative to the size of the object. To potentially allow comparisons among different robotic grippers in terms of their grasping capabilities under pose uncertainties, Fig. 19 also provides nondimensionalized values (shown in blue), i.e., the results divided by the length of the finger projected on the plane, $L(= 9.2$ cm).

VI. Conclusion

A. Discussion

This article presented a new underactuated robotic gripper based on the origami-inspired 3-D-printed mechanism. The new CAD design method combined with a different soft material improved durability and structural stiffness, compared with the previous model. Despite such improvements, we identified several limitations yet to be addressed. The 3-D-printed structures are still not durable enough for a long-term use in real-world applications. The current prototype was fabricated and continuously used in experiments over the past three months, and the fingers exhibited reduced flexibility and small cracks over this period. The stiffness and fatigue properties of the printed structure were also highly sensitive to ambient temperature and humidity. For example, when exposed in cold temperature and dry air, the structure became stiffer and more susceptible to fractures; on the other hand, when the air in the surrounding was warm and humid, the structure became more flexible, increasing its overall durability but decreasing its stiffness and load bearing capacity. Such limitations were directly related to the design and materials used for fabrication, which were also observed in Fig. 8. In particular, materials used for the soft components play a significant role in durability and overall mechanical and dynamic properties of the printed structures. Currently, only two most flexible materials from the list of materials provided by the manufacturer were tested; further investigation on various materials and engineering new optimally designed materials must be followed.

B. Potential

Compliant underactuated robots have great potential to address unmet needs of traditional rigid robots, such as frequent physical interactions with the environment (or humans) and manipulation of fragile or irregular objects. However, there lacks design methods, which allow customized design of compliant or soft mechanisms, which would exhibit desired structural and dynamic properties. Most of the existing robots have their own unique designs, which are not applicable for other types of robots or those in different physical sizes. The presented mechanism design is highly customizable and, thus, can be used for broad robotics applications. While the structural geometry may appear to be relatively complex, the design principles are simple (and thus easy to customize), and the structural complexity does not affect the fabrication complexity or time as it is designed for 3-D printing.

This underactuated robotic gripper using the presented compliant mechanism has great potential for applications in robotic manufacturing and human–robot collaboration. Unlike most industrial robots designed for precise repetitive manipulations of identical objects, the demonstrated grasping capability can significantly lower the sensing resolution and, thus, reduce the control complexity and processing time when handling irregular objects. The inherent compliance in the robots made of the TWISTER mechanisms would be well suited for direct human–robot interaction and collaborative task performance. To focus on the grasping performance of the origami-inspired 3-D-printed fingers, we did not add additional fingertip structures. Different fingertip designs can help better acquisition of objects and, thus, improve overall grasping performance of TWISTER Hand.

Further investigation on materials, design, and functional properties will continue in order to fully establish this new

design as a customizable robotic mechanism. In addition, the current form of the robot embodiment aims to demonstrate its sensorless, dexterous, and compliant manipulation capability using a minimum number of actuator(s). The three fingers were simultaneously actuated for closing and opening by pulling and releasing the cables connected to a single servo motor. Therefore, the configurational capabilities of TWISTER are significantly underutilized. By using more than one actuator, TWISTER Hand can exhibit more diverse dexterous manipulation capabilities, which has yet to be explored.

APPENDIX

Table III lists 36 objects used in our experiments. For each object, its weight (N) and overall dimensions (mm^3) are also provided.

TABLE III
LIST OF 36 OBJECTS USED IN THE GRASPING EXPERIMENTS

Name of Object	Weight (N)	Length×Height×Width (mm^3)
Combos snack	0.54	137 × 72 × 30
Planters snack	0.88	143 × 80 × 30
M&M snack	0.46	137 × 62 × 23
Lime	1.06	63 × 56 × 56
Clementine	0.81	50 × 59 × 59
Cube	0.07	38 × 38 × 38
Mentos snack	0.4	90 × 38 × 26
Egg shell	0.05	62 × 42 × 42
Water sprayer	0.45	160 × 83 × 83
Electric tape	0.15	15 × 56 × 56
Screw driver	0.47	90 × 30 × 30
Banana	1.65	200 × 45 × 45
Large wire spool	0.96	82 × 90 × 90
Medium wire spool	1.86	60 × 55 × 55
Small wire spool	0.23	20 × 55 × 55
Double-sided tape	1.17	19 × 118 × 118
Wire glue contrainer	0.22	31 × 34 × 34
Wireless mouse	0.82	94 × 55 × 39
Wired mouse	0.97	123 × 61 × 40
TWISTER finger	0.12	130 × 25 × 29
Scissors	0.74	215 × 80 × 20
Plastic bottle	0.25	160 × 55 × 55
Digital watch	0.72	80 × 51 × 51
Spring clamp	1.29	155 × 85 × 40
Boiled egg	0.64	58 × 45 ×45
Rubik's cube	1.05	57 × 57 × 57
Piece of fabric	0.06	0.2 × 156 × 200
White bear toy	0.39	110 × 125 × 100
Unicorn toy	0.4	185 × 85 × 105
Teddy bear	0.52	180 × 160 × 95
Clear plastic cup	0.09	102 × 68 × 68
Brown paper cup	0.13	105 × 60 × 78
White styrofoam Cup	0.05	94 × 59 × 59
Eraser	0.27	65 × 25 × 13
Pencil	0.05	185 × 7 × 7
Yogurt cup	1.59	57 × 86 × 86

REFERENCES

[1] D. Jeong and K. Lee, "OrigamiBot-II: An amphibious robot with reconfigurable origami wheels for locomotion in dynamic environments," in *Proc. ASME Int. Mech. Eng. Congr. Expo.*, vol. 4A: Dynamics, Vibration, and Control. Houston, Texas, USA, Nov. 13–19, 2015, Paper V04AT04A026, ASME.

[2] E. VanderHoff, D. Jeong, and K. Lee, "OrigamiBot-I: A thread-actuated origami robot for manipulation and locomotion," in *Proc. IEEE/RSJ Int. Conf. Intell. Robots Syst.*, 2014, pp. 1421–1426.

[3] D. Jeong and K. Lee, "Design and analysis of an origami-based three-finger manipulator," *Robotica*, vol. 36, no. 2, pp. 261–274, 2018.

[4] D.J. Balkcom and M. T. Mason, "Robotic origami folding," *Int. J. Robot. Res.*, vol. 27, no. 5, pp. 613–627, 2008.

[5] K. Tanaka, Y. Kamotani, and Y. Yokokohji, "Origami folding by a robotic hand," in *Proc. IEEE/RSJ Int. Conf. Intell. Robots Syst.*, 2007, pp. 2540–2547.

[6] T. Liu, Y. Wang, and K. Lee, "Three-dimensional printable origami twisted tower: Design, fabrication, and robot embodiment," *IEEE Robot. Autom. Lett.*, vol. 3, no. 1, pp. 116–123, Jan. 2018.

[7] Y. Wang and K. Lee, "3D-printed semi-soft mechanisms inspired by origami twisted tower," in *Proc. NASA/ESA Conf. Adaptive Hardware Syst.*, 2017, pp. 161–166.

[8] M. Schenk and S. D. Guest, "Origami folding: A structural engineering approach," in *Proc. 5th Int. Meet. Origami Sci., Math., Educ.*, 2011, pp. 291–304.

[9] D. Rus and M. T. Tolley, "Design, fabrication and control of origami robots," *Nature Rev. Mater.*, vol. 3, pp. 101–112, 2018.

[10] L. A. Bowen, C. L. Grames, S. P. Magleby, L. L. Howell, and R. J. Lang, "A classification of action origami as systems of spherical mechanisms," *J. Mech. Des.*, vol. 135, no. 11, 2013, Art. no. 111008.

[11] G. Wei and D. Jian, "Origami-inspired integrated planar-spherical overconstrained mechanisms," *J. Mech. Des.*, vol. 136, no. 5, 2014, Art. no. 051003.

[12] M. Salerno, K. Zhang, A. Menciassi, and J. S. Dai, "A novel 4-DOF origami grasper with an SMA-actuation system for minimally invasive surgery," *IEEE Trans. Robot.*, vol. 32, no. 3, pp. 484–498, Jun. 2016.

[13] K. Kuribayashi *et al.*, "Self-deployable origami stent grafts as a biomedical application of Ni-rich TiNi shape memory alloy foil," *Mater. Sci. Eng.: A*, vol. 419, no. 1, pp. 131–137, 2006.

[14] H. Okuzaki, T. Saido, H. Suzuki, Y. Hara, and H. Yan, "A biomorphic origami actuator fabricated by folding a conducting paper," *J. Phys.: Conf. Ser.*, vol. 127, no. 1, 2008, Art. no. 012001.

[15] R. Martinez, F. Carina, X. Chen, and W. George, "Elastomeric origami: Programmable paper-elastomer composites as pneumatic actuators," *Adv. Funct. Mater.*, vol. 22, no. 7, pp. 1376–1384, 2012.

[16] S. J. Kim, D. Y. Lee, G. P. Jung, and K. J. Cho, "An origami-inspired, self-locking robotic arm that can be folded flat," *Sci. Robot.*, vol. 3, no. 16, 2018, Art. no. eaar2915.

[17] F. Zuliani, C. Liu, J. Paik, and S. M. Felton, "Minimally actuated transformation of origami machines," *IEEE Robot. Autom. Lett.*, vol. 3, no. 3, pp. 1426–1433, Jul. 2018.

[18] Y. Chen, H. Feng, J. Ma, R. Peng, and Z. You, "Symmetric waterbomb origami," *Proc. Roy. Soc. A*, vol. 472, no. 2190, 2016, Art. no. 20150846.

[19] D. Lee, J. S. Kim, J. J. Park, S. R. Kim, and K. J. Cho, "Fabrication of origami wheel using pattern embedded fabric and its application to a deformable mobile robot," in *Proc. IEEE Int. Conf. Robot. Autom.*, 2014, pp. 2565–2565.

[20] D. Y. Lee, J. S. Kim, S. R. Kim, J. S. Koh, and K. J. Cho, "The deformable wheel robot using magic-ball origami structure," in *Proc. ASME Int. Des. Eng. Tech. Conf. Comput. Inf. Eng. Conf.*, 2013, Art. no. V06BT07A040.

[21] X. Liu, S. Yao, S. V. Georgakopoulos, B. S. Cook, and M. M. Tentzeris, "Reconfigurable helical antenna based on an origami structure for wireless communication system," *Proc. IEEE Int. Microw. Symp.*, 2014, pp. 1–4.

[22] G. Ayes, Y. Liu, J. Genzer, G. Lazzi, and M. D. Dickey, "Self-folding origami microstrip antennas," *IEEE Trans. Antennas Propag.*, vol. 62, no. 10, pp. 5416–5419, Oct. 2014.

[23] I. Nam, G. P. Kim, S. Park, J. W. Han, and J. Yi, "All-solid-state, origami-type foldable supercapacitor chips with integrated series circuit analogues," *Energy Environ. Sci.*, vol. 7, no. 3, pp. 1095–1102, 2014.

[24] S. Miyashita, L. Meeker, T. Tolley, J. Wood, and D. Rus, "Self-folding miniature elastic electric devices," *Smart Mater. Struct.*, vol. 23, no. 9, 2014, Art. no. 094005.

[25] M. De Temmerman, M. Mollaert, T. Van Mele, and L. De Laet, "Design and analysis of a foldable mobile shelter system," *Int. J. Space Struct.*, vol. 22, no. 3, pp. 161–168, 2007.

[26] J. Ma and Z. You, "The Origami Crash Box," in *Origami 5: Fifth International Meeting of Origami Science, Mathematics, and Education*. New York, NY, USA: Taylor & Francis, 2011, pp. 277–290.

[27] J. Ma and Z. You, "A novel origami crash box with varying profiles," in *Proc. Int. Des. Eng. Tech. Conf. Comput. Inf. Eng. Conf.*, 2013, Art. no. V06BT07A048.

[28] S. S. Tolman, I. L. Delimont, L. L. Howell, and D. T. Fullwood, "Material selection for elastic energy absorption in origami-inspired compliant corrugations," *Smart Mater. Struct.*, vol. 23, no. 9, 2014, Art. no. 094010.

[29] P. H. Le, J. Molina, and S. Hirai, "Application of Japanese origami ball for floating multirotor aerial robot," *World Acad. Sci., Eng. Technol., Int. J. Mech., Aerosp., Ind., Mechatronic Manuf. Eng.*, vol. 8, no. 10, pp. 1740–1743, 2014.
[30] P. H. Le, Z. Wang, and S. Hirai, "Origami structure toward floating aerial robot," in *Proc. IEEE Int. Conf. Adv. Intell. Mechatronics*, 2015, pp. 1565–1569.
[31] C. D. Onal, M. T. Tolley, R. J. Wood, and D. Rus, "Origami-inspired printed robots," *IEEE/ASME Trans. Mechatronics*, vol. 20, no. 5, pp. 2214–2221, Oct. 2015.
[32] S. M. Felton, M. T. Tolley, C. D. Onal, D. Rus, and R. J. Wood, "Robot self-assembly by folding: A printed inchworm robot," in *Proc. IEEE Int. Conf. Robot. Autom.*, 2013, pp. 277–282.
[33] S. M. Felton, M. T. Tolley, E. Demaine, D. Rus, and R. J. Wood, "A method for building self-folding machines," *Science*, vol. 345, no. 6197, pp. 644–646, 2014.
[34] J. K. Paik, A. Byoungkwon, D. Rus, and R. J. Wood, "Robotic origamis: Self-morphing modular robot," in *Proc. Int. Comput. Music Conf.*, 2012, Art. no. EPFL-CONF-206919.
[35] W. Gao, K. Huo, J. S. Seehra, K. Ramani, and R. J. Cipra, "HexaMorph: A reconfigurable and foldable hexapod robot inspired by origami," in *Proc. IEEE/RSJ Int. Conf. Intell. Robots Syst.*, 2014, pp. 4598–4604.
[36] S. Seok, C. D. Onal, R. Wood, D. Rus, and S. Kim, "Peristaltic locomotion with antagonistic actuators in soft robotics," in *Proc. Int. Conf. Robot. Autom.*, 2010, pp. 1228–1233.
[37] M. E. Giannaccini *et al.*, "A variable compliance, soft gripper," *Auton. Robots*, vol. 36, nos. 1/2, pp. 93–107, 2014.
[38] M. Cianchetti, M. Follador, B. Mazzolai, P. Dario, and C. Laschi, "Design and development of a soft robotic octopus arm exploiting embodied intelligence," in *Proc. IEEE Int. Conf. Robot. Autom.*, 2012, pp. 5271–5276.
[39] E. Brown *et al.*, "Universal robotic gripper based on the jamming of granular material," *Proc. Nat. Acad. Sci.*, vol. 107, no. 44, pp. 18809–18814, 2010.
[40] J. R. Amend, E. Brown, N. Rodenberg, H. M. Jaeger, and H. Lipson, "A positive pressure universal gripper based on the jamming of granular material," *IEEE Trans. Robot.*, vol. 28, no. 2, pp. 341–350, Apr. 2012.
[41] C. Liu *et al.*, "Optimal design of a soft robotic gripper for grasping unknown objects," *Soft Robot.*, vol. 5, no. 4, pp. 452–465, 2018.
[42] R. Deimel and O. Brock, "A novel type of compliant and underactuated robotic hand for dexterous grasping," *Int. J. Robot. Res.*, vol. 35, nos. 1–3, pp. 161–185, 2016.
[43] F. Ilievski, A. D. Mazzeo, R. F. Shepherd, X. Chen, and G. M. Whitesides, "Soft robotics for chemists," *Angewandte Chemie*, vol. 123, no. 8, pp. 1930–1935, 2011.
[44] B. S. Homberg, R. K. Katzschmann, M. R. Dogar, and D. Rus, "Haptic identification of objects using a modular soft robotic gripper," in *Proc. IEEE/RSJ Int. Conf. Intell. Robots Syst.*, 2015, pp. 1698–1705.
[45] G. Udupa, P. Sreedharan, P. Sai Dinesh, and D. Kim, "Asymmetric bellow flexible pneumatic actuator for miniature robotic soft gripper," *J. Robot.*, vol. 2014, 2014, Art. no. 902625.
[46] S. Wakimoto, K. Ogura, K. Suzumori, and Y. Nishioka, "Miniature soft hand with curling rubber pneumatic actuators," in *Proc. IEEE Int. Conf. Robot. Autom.*, 2009, pp. 556–561.
[47] B. S. Homberg, R. K. Katzschmann, M. R. Dogar, and D. Rus, "Robust proprioceptive grasping with a soft robot hand," *Auton. Robots*, vol. 43, pp. 681–696, 2018.
[48] E. Khaled, G. Neumann, S. Pearson, M. Jackson, and N. Lohse, "Contact detection and size estimation using a modular soft gripper with embedded flex sensors," in *Proc. IEEE/RSJ Int. Conf. Intell. Robots Syst.*, 2018, pp. 498–503.
[49] Y. Fei, J. Wang, and W. Pang, "A novel fabric-based versatile and stiffness-tunable soft gripper integrating soft pneumatic fingers and wrist," *Soft Robot.*, vol. 6, pp. 1–20, 2018.
[50] P. Glick, S. A. Suresh, D. Ruffatto, M. Cutkosky, M. T. Tolley, and A. Parness, "A soft robotic gripper with gecko-inspired adhesive," *IEEE Robot. Autom. Lett.*, vol. 3, no. 2, pp. 903–910, Apr. 2018.
[51] H. Zhang, A. S. Kumar, J. Fuh, and M. Wang, "Investigation on developing a topology optimized and 3D printable multimaterial soft gripper," in *Proc. IEEE 14th Int. Conf. Control Autom.*, 2018, pp. 692–697.
[52] H. Zhang, A. S. Kumar, J. Fuh, and M. Wang, "Topology optimized design, fabrication and evaluation of a multimaterial soft gripper," in *Proc. IEEE Int. Conf. Soft Robot.*, 2018, pp. 424–430.
[53] H. Dong, E. Asadi, C. Qiu, J. Dai, and I. M. Chen, "Geometric design optimization of an under-actuated tendon-driven robotic gripper," *Robot. Comput.-Integr. Manuf.*, vol. 50, pp. 80–89, Apr. 2018.
[54] A. Agarwal, V. Viswanathan, S. Maheshwari, and P. V. Alvarado, "Effects of material properties on soft gripper grasping forces," in *Proc. IEEE Int. Conf. Soft Robot.*, 2018, pp. 437–442.
[55] A. K. Mishra, E. D. Dottore, A. Sadeghi, A. Mondini, and B. Mazzolai, "SIMBA: Tendon-driven modular continuum arm with soft reconfigurable gripper," *Front. Robot. AI*, vol. 4, 2017, Art. no. 4.
[56] T. Hassan, M. Manti, G. Passetti, N. d'Elia, M. Cianchetti, and C. Laschi, "Design and development of a bio-inspired, under-actuated soft gripper," in *Proc. 37th Annu. Int. Conf. IEEE Eng. Med. Biol. Soc.*, 2015, pp. 3619–3622.
[57] A. M. Dollar and R. D. Howe, "Towards grasping in unstructured environments: Grasper compliance and configuration optimization," *Adv. Robot.*, vol. 19, no. 5, pp. 523–543, 2005.
[58] A. M. Dollar and R. D. Howe, "The highly adaptive SDM hand: Design and performance evaluation," *Int. J. Robot. Res.*, vol. 29, no. 5, pp. 585–597, 2010.
[59] G. A. Kragten, M. Baril, C. Gosselin, and J. L. Herder, "Stable precision grasps by underactuated grippers," *IEEE Trans. Robot.*, vol. 27, no. 6, pp. 1056–1066, Dec. 2011.
[60] D. Aukes, S. Kim, P. Garcia, A. Edsinger, and M. R. Cutkosky, "Selectively compliant underactuated hand for mobile manipulation," in *Proc. IEEE Int. Conf. Robot. Autom.*, 2012, pp. 2824–2829.
[61] D. M. Aukes *et al.*, "Design and testing of a selectively compliant underactuated hand," *Int. J. Robot. Res.*, vol. 33, no. 5, pp. 721–735, 2014.
[62] L. U. Odhner *et al.*, "A compliant, underactuated hand for robust manipulation," *Int. J. Robot. Res.*, vol. 33, no. 5, pp. 736–752, 2014.
[63] Materials Data Sheet. [Online]. Available: http://www.stratasys.com/materials/material-safety-data-sheets/polyjet

Kiju Lee received the B.S.E. degree in electrical and electronics engineering from Chung-Ang University, Seoul, South Korea, in 2002, and the M.S.E. and Ph.D. degrees in mechanical engineering from Johns Hopkins University, Baltimore, MD, USA, in 2006 and 2008, respectively.

From 2008 to 2019, she was with the Department of Mechanical and Aerospace Engineering, Case Western Reserve University, Cleveland, OH, USA. Since 2019, she has been with the Department of Engineering Technology and Industrial Distribution and the Department of Mechanical Engineering, Texas A&M University, College Station, TX, USA. She is the Director of the Adaptive Robotics and Technology Lab, through which she runs various research projects focusing on novel robotic mechanism design, tangible game technologies, and swarm robotics.

Yanzhou Wang received the B.S. degree in mechanical engineering from Case Western Reserve University, Cleveland, OH, USA, in 2019. He is currently working toward the M.S.E. degree in mechanical engineering with Johns Hopkins University, Baltimore, MD, USA.

His research interests include origami-inspired robotics, soft robotics, medical robotics, and mechanism design.

Chuanqi Zheng received the B.S. degree in welding technology and engineering and the M.S. degree in materials engineering from the Harbin Institute of Technology, Harbin, China, in 2012 and 2014, respectively. He is currently working toward the Ph.D. degree in mechanical engineering with Texas A&M University, College Station, TX, USA.

His research interests include robot mechanism design and control.